# Characterizing the evolution of mass flow properties and dynamics through analysis of seismic signals: Insights from the 18 March 2007 Mt. Ruapehu lake-breakout lahar

Braden Walsh[1], Charline Lormand[2], Jon Procter[3], Glyn Williams-Jones[1]

[1]Department of Earth Sciences, Simon Fraser University, Burnaby, British Columbia, Canada

[2]Department of Earth Sciences, University of Durham, Durham, DH1 3LE, UK

[3]Volcanic Risk Solutions, Institute of Agriculture and Environment, Massey University, Palmerston North, New Zealand

Corresponding Author: Braden Walsh (braden_walsh@sfu.ca)

## Abstract

Monitoring for mass flows on volcanoes can be challenging due to the ever-changing landscape along the flow path, which can drastically transform the properties and dynamics of the flow. These changes to the flows require the need for detection strategies and risk assessment that are tailored not only between different volcanoes, but at different distances along flow paths as well. Being able to understand how a flow event may transform in time and space along the channel is of utmost importance for hazard management. While visual observations and simple measuring devices in the past have shown how volcanic mass flows transform along the flow

path, these same features for the most part have not been described using seismological methods. On 18 March 2007, Mt. Ruapehu produced the biggest lahar in New Zealand in over 100 years. At 23:18 UTC the tephra dam holding the Crater Lake water back collapsed causing $1.3x10^6$ $m^3$ of water to flow out and rush down the Whangaehu channel. We describe here the seismic signature of a lake-breakout lahar over the course of 83 km along the Whangaehu river system using three 3-component broadband seismometers installed <10 m from the channel at 7.4, 28, and 83 km from the crater lake source. Examination of 3-component seismic amplitudes, frequency content, and directionality, combined with video imagery and sediment concentration data were used. The seismic data shows the evolution of the lahar as it transformed from a highly turbulent out-burst flood (high peak frequency throughout), to a fully bulked up multi-phase hyperconcentrated flow (varying frequency patterns depending on the lahar phase) to a slurry flow (bedload dominant). Estimated directionality ratios show the elongation of the lahar with distance down channel, where each recording station depicts a similar pattern, but for differing lengths of time. Furthermore, using directionality ratios shows extraordinary promise for lahar monitoring and detection systems where streamflow is present in the channel.

## 1. Introduction

Volcanic mass flows (e.g. debris flows, pyroclastic density currents, debris avalanches, hyperconcentrated flows) are one of the greatest threats to communities, industry, recreation, etc. on and around volcanoes. Volcanic mass flows are particularly dangerous as they are fast moving turbulent flows that can occur without any warning or an eruption transpiring (Capra et

al., 2010). These flows can move a sizable amount of liquid and debris great distances that can critically impact locations hundreds of kilometers from the volcano or source. Lake-breakout or outburst flood events can be particularly destructive because they tend to be larger and can cause long lasting changes to the landscape and surrounding ecosystems (O'Connor et al., 2013; Procter et al., 2021). Furthermore, unlike eruption or rain triggered mass flows, outburst floods have very little to no warning. Eruption triggered flows can be prepared for by the onset of the eruption and/or the monitoring of the volcano through various methods (e.g. seismology, infrasound, gravity, gas and water chemistry). Likewise, for rain-induced flows using techniques such as measuring the amount or intensity of rain (e.g. Capra et al., 2010; 2018) or by monitoring the amount of available material (e.g. Iguchi, 2019) can help forecast when an event may occur.

In New Zealand, there have been numerous cases of large damaging mass flows in modern times. For example, in October 2012, a lake-breakout lahar originating from Te Maari, destroyed hiking trails and forestry, eventually flowing over 4.5 km to damage and block off Highway 46 (Procter et al., 2014; Walsh et al., 2016). Moreover, on 24 December 1953, the deadliest volcanic mass flow in New Zealand history occurred killing 151 people when a lahar struck a train crossing at the Tangiwai Rail Bridge, 39.8 km from the Crater Lake on top of Mt. Ruapehu (O'Shea, 1954). The ability to predict and investigate the changing dynamics and properties of large volcanic mass flows as they progress down channel is the first step in beginning to understand flow mechanisms better, and ultimately address the hazards involved to mitigate the risk.

In order to better characterize and understand these flow events, many in-situ applications and instruments have been used in the past (e.g. trip wires, stage gauge, load cells, pore pressure). While many of these tools can yield quick assessments and provide ample warning (e.g. current meters, trip wires), they can sometimes be at risk of false detections, equipment damage or loss, and/or lack the capability to evaluate multiple pulses or flow events (Arattano et al., 1999). Geophysical instruments (e.g. seismometers, geophones, infrasound) on the other hand can be installed at a safe distance away from the channel and have shown signs of not only being capable warning systems (e.g. Coviello et al., 2019), but have the ability to accurately estimate flow properties (e.g. Arattano and Marchi, 2005; Doyle et al., 2010; Schimmel et al., 2021), as well as flow dynamics (e.g. Gimbert et al., 2014; Coviello et al., 2018; Walsh et al., 2020). However, in order to fully utilize these instruments, improved interpretation, comprehension, assessment, and universality is needed. One technique to increase the ability to predict, warn, and estimate the properties and dynamics of flow events is to use all three components of the seismic recording. Recently, several studies have shown that using all three components is effective in characterizing flow events (e.g. snow-slurry lahars, Cole et al., 2009; snow avalanches, Kogelnig et al., 2011; streamflow, Roth et al., 2016; landslides, Surinach et al., 2005; lahars, Walsh et al., 2020; rockfalls, Kuehnert et al., 2021; hyperconcentrated flows, Walsh et al., 2016). Using the horizontal components along with the vertical component can yield additional information about the flow that is not utilized if only the vertical component is used. Notably, directionality (cross-channel over channel-parallel) analysis (e.g. Doyle et al., 2010; Walsh et al., 2020) can provide information about the wetted perimeter, sediment concentration, and number of particle collisions. Furthermore, differing energies and frequency

outputs from channel parallel and channel perpendicular signals can point to specific changes within the flow (Burtin et al., 2010; Roth et al., 2016) that can provide insights into the internal dynamics.

### 1.1 Anatomy of lahars

When a lahar is created from a lake-breakout or outburst flood event, the transition from flood or streamflow torrent depends on the erosivity of the channel and the supply of sediment being entrained within the flow (e.g. Scott, 1988; Doyle et al., 2011). An event may start as a highly turbulent low sediment flow, then transform into a hyperconcentrated flow, and may even eventually 'bulk up' to exhibit characteristics of a debris flow with the possibility of plug-like (limited internal motion and collisions) or laminar behavior (Scott, 1988, Pierson et al., 1990). At Mt. Ruapehu, the propagational differences of lahars down channel have been observed and characterized in the past (e.g. Cronin et al., 1996; Cronin et al., 1999; Cronin et al., 2000; Manville et al., 2000; Procter et al., 2010a; Lube et al., 2012). From these studies, models of how lahars bulk up and transition throughout the run-out distance have been postulated. For the lahars in the Whangaehu channel, Cronin et al. (1999) created three 4-phase conceptual models based on source distances of 23.5 km, 42 km, and >55 km. The first two models are for lahar regimes, whereas the third model described a lahar almost at its peak run-out distance. In each model, the first phase consists of a super charged streamflow pulse that flows ahead of the head of the flow and is considered the front of the lahar. This phenomenon has also been noted for debris flows interacting with streamflow (Arattano and Moia, 1999). Furthermore, discharge is maximum at the transition between phase 1 and phase 2 (Cronin et al., 1999), and

is described as the head of the flow. Phase 2 is described as a mixing zone between streamflow and increasing sediment content, where the peak sediment concentration usually occurs at the end of phase 2 or at the beginning of phase 3 (e.g. Pierson and Scott, 1985). Cronin et al. (1999) defined phase 3 as the lahar body, which has the least amount of the original streamflow contained within. Phase 3 is also characterized by coarse sediment suspensions and is the most likely location for debris flow rheology. Finally, phase 4 is the tail of the lahar where debulking and dilution occurs transforming the lahar back into a hyperconcentrated, mixed, or streamflow.

### 1.2 18 March 2007 lake-breakout event

Mt. Ruapehu (2797 asl) is the largest stratovolcano in the central North Island of New Zealand (Figure 1) which sits at the southwestern end of the Taupō Volcanic Zone (TVZ). The volcano has a volume of 110 $km^3$ which is composed of several overlapping cone building formations and surrounding ring plain volcaniclastics (Carrivick et al., 2009; Pardo et al., 2012). On top of the volcano, above the currently active vent sits a $1x10^7$ $m^3$ acidic crater lake (Procter et al., 2010a). The Whangaehu channel is the preferred outlet for Crater Lake water and lahars in recent history (Procter et al., 2012; Procter et al., 2021). The Whangaehu channel is on the eastern flank of Mt. Ruapehu where it runs down across the volcanic ring plane and eventually heads southwest for ~200 km reaching the Tasman Sea (Figure 1).

Prior to the events that took place in the morning local time on 18 March 2007, a heavy rainstorm occurred accumulating about 256 mm of water over the 10 hours prior to the dam breach that led to the outburst flood (Massey et al., 2010). The intense rain caused the Crater

126 Lake to rise an extra 6.4 m and overtop the natural lava formation ledge, which started to cause
127 seepage and extra water to enter the Whangaehu gorge (Carrivick et al., 2009). At ~23:18 UTC,
128 the tephra dam collapsed causing $1.3x10^6$ $m^3$ of water to flow out of the lake and into the
129 Whangaehu channel (Procter et al., 2010a). The dam was eroded and undercut in multiple
130 stages resulting in a series of retrogressing landslides along with the main debris flow/lahar.

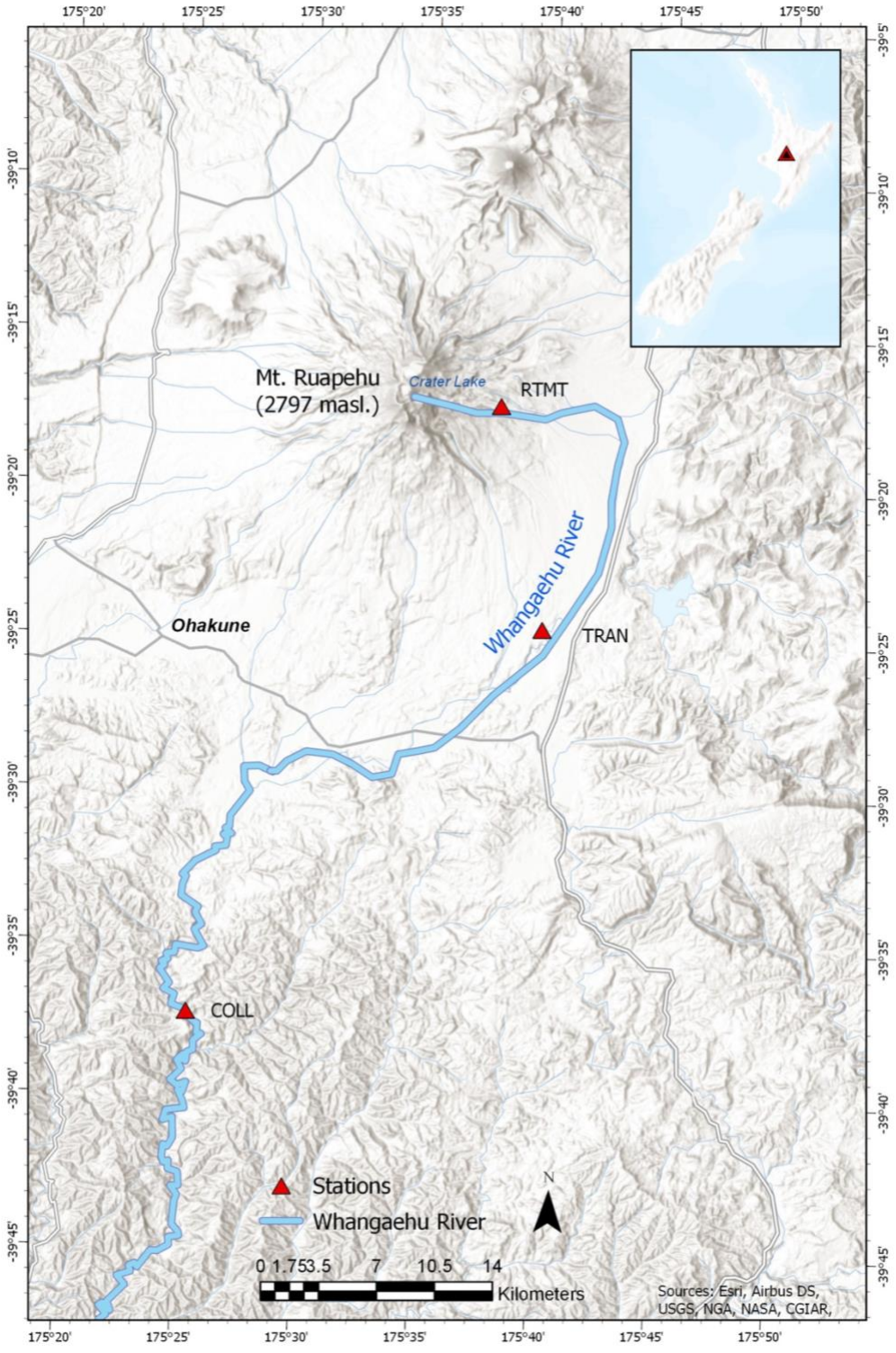


*Figure 1 Map of Mt. Ruapehu and the surrounding area located on the central North Island of New Zealand. Blue outline represents the Whangaehu channel and the path the 18 March 2007 lahar traveled down. Red triangles denotes the three monitoring stations along the Whangaehu channel at 7.4, 28, and 83 km.*

Since the lahar was caused by lake-breakout dynamics and thus contained an abundance of water, the event was classified as a hyperconcentrated streamflow (Procter et al., 2010b). At ~8.0 km from source, the lahar velocity was recorded at ~ 9.5 m/s and had an estimated 6 m of downcutting, showing the capability of the lahar to deposit and erode massive amounts of material (Procter et al., 2010a,b). Furthermore, the 18 March 2007 lahar was one of the most thoroughly monitored lahars ever (Manville and Cronin 2007). In total there were 21 monitoring locations (only three of which had 3-component seismometers) setup to measure various lahar properties, (e.g. flow monitor, camera, stage height, flow sampling, pore-pressure, seismic, etc.) along the channel (Keys and Green, 2008; Lube et al., 2012), with the lahar taking over 16 hours to eventually travel out to the New Zealand coast, ~200 km from the original crater lake source.

Here, we delve into the properties of the 18 March 2007 lake-breakout hyperconcentrated streamflow that bulked up to a volume of ~$4.4 \times 10^6$ $m^3$ (Procter et al., 2010a) over the course of 83 km along the Whangaehu channel, originating from Mt. Ruapehu, New Zealand. The combination of seismic analysis (frequency and directionality) with supplementary measurements (e.g. video, sediment concentration) show how a lahar transforms over time and distance and how using these seismic techniques can help monitor the ever changing dynamics and properties of a flow event. Furthermore, we examine previous models of the evolution of a lahar and compare the model with the seismic data available.

## 2. Data

The seismic data for the 18 March 2007 lahar was recorded on three seismometers installed at various distances (7.4, 28, 83 km) along the Whangaehu channel (Figure 1). The data from the three 3-component broadband Guralp 6T sensors (COLL, RTMT, TRAN) were recorded using a sampling rate of 100 Hz and GPS time stamps. For each site, the seismometers axes were installed to true North and the recorded data were rotated to align North as flow parallel (P) and East as the cross-channel direction (T). The seismic data were rotated to align with the channel in order to determine the differences in energy output between the flow parallel and cross-channel directions (e.g. directionality). The monitoring station Round the Mountain Track (RTMT), was installed 4 m from the channel and 7.4 km downstream from the source of the lahar. The lahar arrived at RTMT at 23:36 UTC and had an average velocity of 9.3 m/s (Figure 2a). The Trans Rail Gauge (TRAN) station was installed 28 km from source and 10 m from the channel, which also included a video camera that captured an image every 30 seconds. The lahar arrived at TRAN at 24:35 UTC and had an average velocity of 5.6 m/s (Figure 2d). The Colliers Bridge (COLL) station was installed 10 m from the channel and 83 km from source. The lahar arrived at COLL at 04:13 UTC and had an average velocity of 4.8 m/s (Figure 2f). Arrival times are based off of images and eye witnesses at each of the monitoring stations. The flow velocity at RTMT and COLL were estimated from imagery and at TRAN from a flow meter. Sediment concentration at COLL was measured manually through dip buckets.

## 3. Results

To examine the multi-component dynamics of the 18 March 2007 lake-breakout event along the Whangaehu channel at three monitoring locations, the data were corrected for instrument

176 response and split into 10 s time windows. At each recording location, peak spectral frequency
177 (PSF), root mean squared (RMS) amplitude, and directionality ratios (DR) are estimated for each
178 of the 10 s time windows (Table S1). At each monitoring station the first hour of the lahar
179 including five minutes prior to the arrival are shown in all the results except when indicated.

180

181

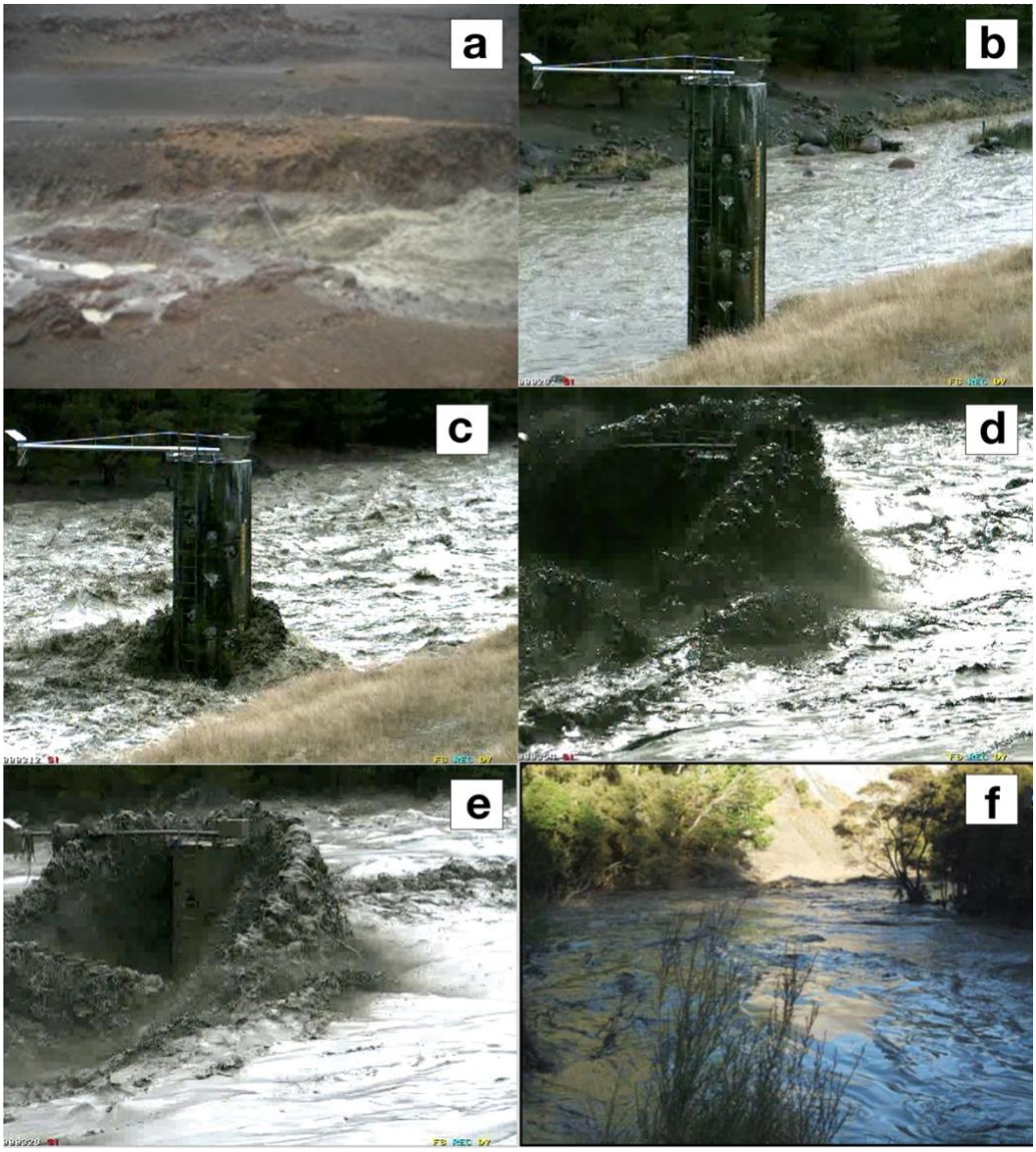


*Figure 2 Images from the 18 March 2007 lake break-out lahar from RTMT (a), TRAN (b, c, d, e), and COLL (f). Note the transformation of the lahar at TRAN from streamflow (b), increased discharge pre-lahar phase 1 pulse/flow front (bow wave) (c), head of the lahar (peak seismic amplitude) (d), and low PSF beginning of lahar body (see figure 4 after 15 minute mark) (e).*

### 3.1 Frequency analysis

In order to examine the PSFs for all three components at each site along the channel, we use the frequency recorded at the maximum amplitude of the frequency spectra for each 10 s running time window (i.e. non-overlapping windowed FFT). The PSF for RTMT (7.4 km from

source) shows similar patterns between all three components (Figure 3). The five minutes prior to the arrival of the front of the lahar are characterized by scattered PSFs between 20-40 Hz for the cross-channel (Figure 3a) and parallel (Figure 3b) directions, while in the vertical direction (Figure 3c) the PSF is ~30 Hz. When the front (streamflow pulse/bow wave) of the lahar arrives at the station, the PSF in all three components decreases to ~5-10 Hz for about 1 min before increasing again to higher frequencies. After the head (peak seismic amplitude) of the lahar passes the station, the PSF in the cross-channel and parallel directions remain between 30-40 Hz for the rest of the recording window. In the vertical component, the PSF is scattered between 20-40 Hz for ~15 min after the arrival of the head of the lahar and then becomes narrower, similar to both the cross-channel and parallel components with PSFs between 30-40 Hz.

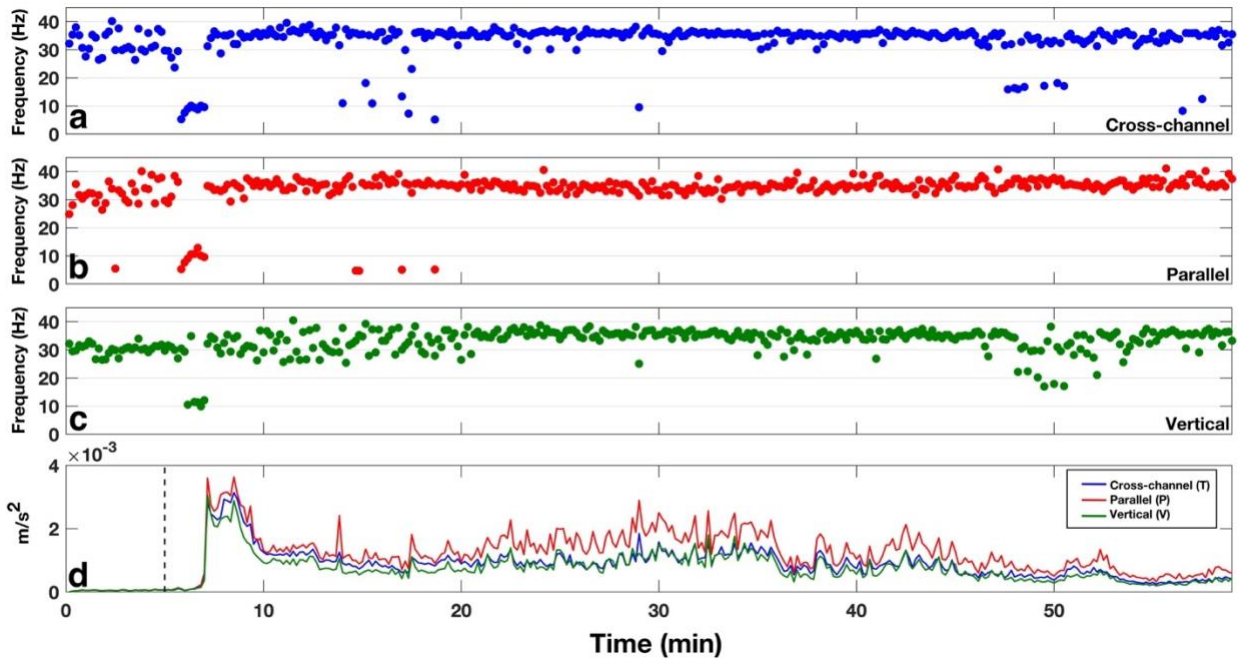


*Figure 3 Peak spectral frequencies for RTMT (7.4 km from source) for a) cross-channel (blue), b) flow parallel (red), and c) vertical (gree) directions. Bottom row (d) depicts the RMS amplitude of the lahar color coded to the same*

*colors as the PSF. The dashed vertical line marks the timing of the lahar front passing the monitoring station. All PSFs and RMS amplitudes were calculated using 10 s time windows.*

Further down the channel at station TRAN (28 km from source), the PSFs for all three components show a similar overall pattern (Figure 4). The pre-lahar PSF distribution in all three components is between 20-32 Hz. Like RTMT higher up the channel, the PSFs for the front of the lahar at TRAN drops down to around 10 Hz and when the lahar head arrives (~10 min, Figure 4) the PSF increases to ~30 Hz for parallel (Figure 4b) and cross-channel (Figure 4a) directions and between 20-30 Hz in the vertical component (Figure 4c). This decrease to lower frequencies before the head of the lahar at TRAN lasts for about 5 min. After the head of the lahar passes the recording station the PSF content decreases for ~15 min to 10-20 Hz for the parallel and cross-channel components and between 10-25 Hz for the vertical components. The PSF after the 30 minute mark in Figure 4 displays a bimodal pattern with frequencies between 10-35 Hz, with PSF time windows concentrating most at ~30 Hz.

At the COLL recording station (83 km from source), the PSF distribution shows differing patterns for all three components (Figure 5). The PSF in the cross-channel direction (Figure 5a) depicts a bimodal pattern throughout with a strong lower concentration of time windows at ~18 Hz and a higher PSF at ~25 Hz. For the parallel component (Figure 5b), the pre-lahar signal has a wide PSF range between 12-30 Hz. When the lahar arrives, the PSF becomes concentrated at ~22 Hz for ~8 min before transforming into a bimodal pattern similar to that of the cross-channel PSF, with frequencies between 20-30 Hz. In the vertical component (Figure 5c), the pre-lahar PSF is scattered between 22-30 Hz, then as the front of the lahar passes the station, the PSF stabilizes around 28 Hz for about 12 min. When the lahar head arrives, the PSF again transitions to more of a scattered pattern during the highest energy stage of the lahar (Figure 5, 25-40 min).

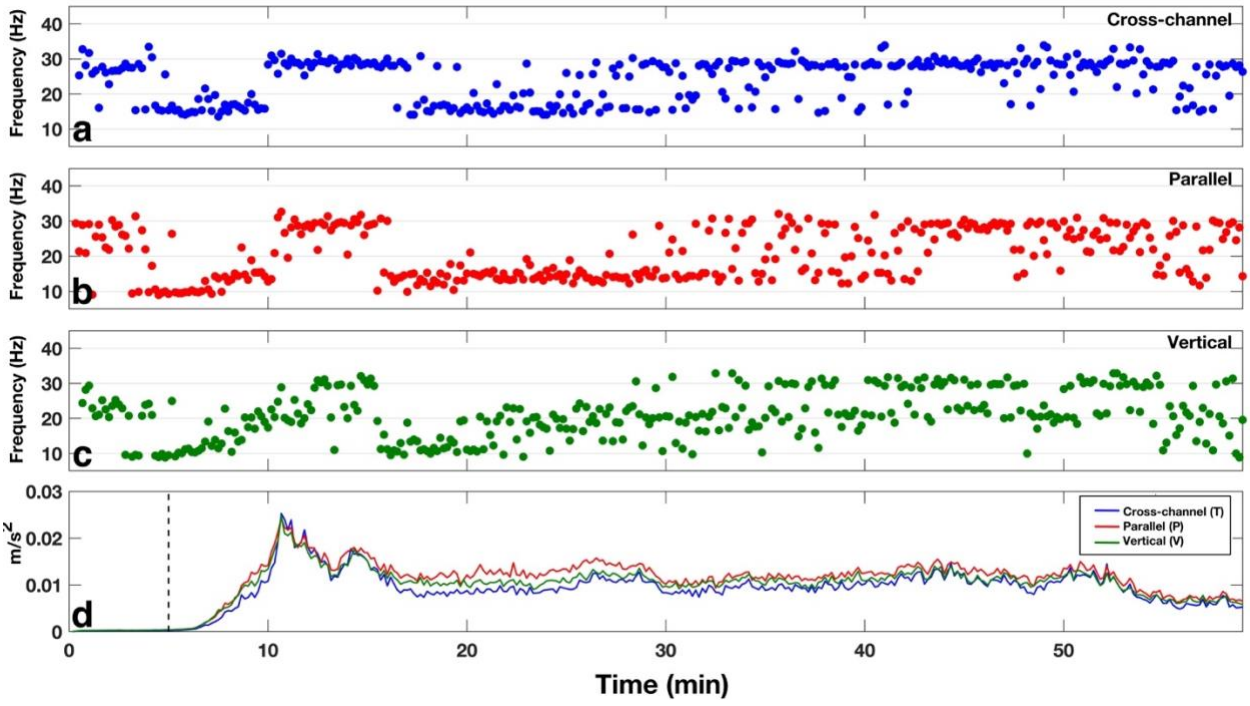


*Figure 4 Peak spectral frequencies for TRAN (28 km from source) for a) cross-channel (blue), b) flow parallel (red), and c) vertical (green) directions. Bottom row (d) depicts the RMS amplitude of the lahar color coded to the same colors as the PSF. The dashed vertical line marks the timing of the lahar front passing the monitoring station. All PSFs and RMS amplitudes were calculated using 10 s time windows.*

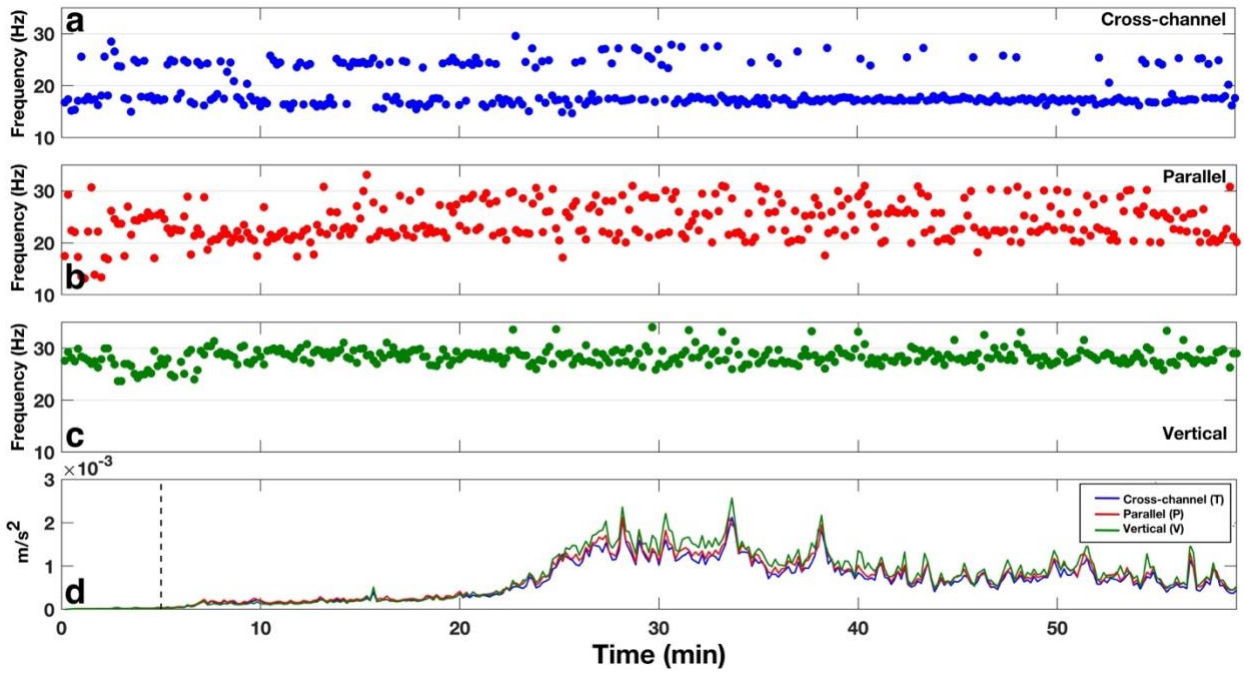


*Figure 5 Peak spectral frequencies for COLL (83 km from source) for a) cross-channel (blue), b) flow parallel (red), and c) vertical (green) directions. Bottom row (d) depicts the RMS amplitude of the lahar color coded to the same colors as the PSF. The dashed vertical line marks the timing of the lahar front passing the monitoring station. All PSFs and RMS amplitudes were calculated using 10 s time windows.*

### 3.2 Directionality

When recording mass flows with 3-component sensors, the directionality may be examined due to the sensor being able to record signals in the two horizontal directions. The directionality ratio allows for the determination of which horizontal component has stronger energy over the course of the recording window. This is possible because, in channel side deployments for mass flow monitoring systems, the sensor is either installed so that the North component is aligned to be parallel and the East component aligned as perpendicular to the flow, or the components are rotated during the data processing stage to align with the channel orientation. Furthermore, with the channel side installations, attenuational factors can mostly be ignored due to the close proximity to the channel and energy output of the flow event. The

249 directionality ratio (DR) can be defined as the cross-channel amplitude divided by the flow
250 parallel amplitude. A DR > 1 indicates that the cross-channel amplitude is larger than that of the
251 flow parallel, and vice-versa for a DR < 1. Directionality ratios have been used in the past to
252 show rheology changes within flows, where the DR increases when streamflow transitions into
253 a lahar (Walsh et al., 2020), and have been hypothesized to be an indicator for flow properties
254 such as, sediment concentration, wetted perimeter, and/or amount of particle collisions within
255 a lahar (Doyle et al., 2010).

256 The directionality ratios estimated from 10 s non-overlapping running time windows of the RMS
257 amplitudes at each seismic station for the 18 March 2007 lake-breakout lahar are shown in
258 Figure 6. The DR for RTMT (Figure 6a) displays a DR <= 1 (0.8-1.0) pre-lahar, then decreases
259 (0.7-0.8) as the lahar arrives at the recording station (Figure 6, dashed line), then as soon as the
260 lahar head arrives, the DR increases to above DR = 1 for ~2 min. After the peak lahar flood pulse
261 passes RTMT, the DR then proceeds to decrease below a DR = 1 for the rest of the recording
262 window. Similar to RTMT, the DR for TRAN starts out with a DR < 1 (0.7-0.8) and as the lahar
263 front passes, the DR similarly decreases to 0.6-0.7 before increasing to a DR > 1 for ~5 min
264 when the lahar is at peak energy output starting at about the 10 min mark (Figure 6d, red line).
265 After the passing of the peak energy, the DR for TRAN decreases below 1 again for the
266 remainder of the recording window. Further down the channel at COLL (Figure 6c), the DR
267 before the lahar arrives has a wide range of values between 0.8-1.2. When the front of the
268 lahar passes (Figure 6, dashed line), the DR stabilizes between 0.8-1, before increasing slightly
269 when the peak energy of the lahar passes the monitoring site at about the 25 min mark.

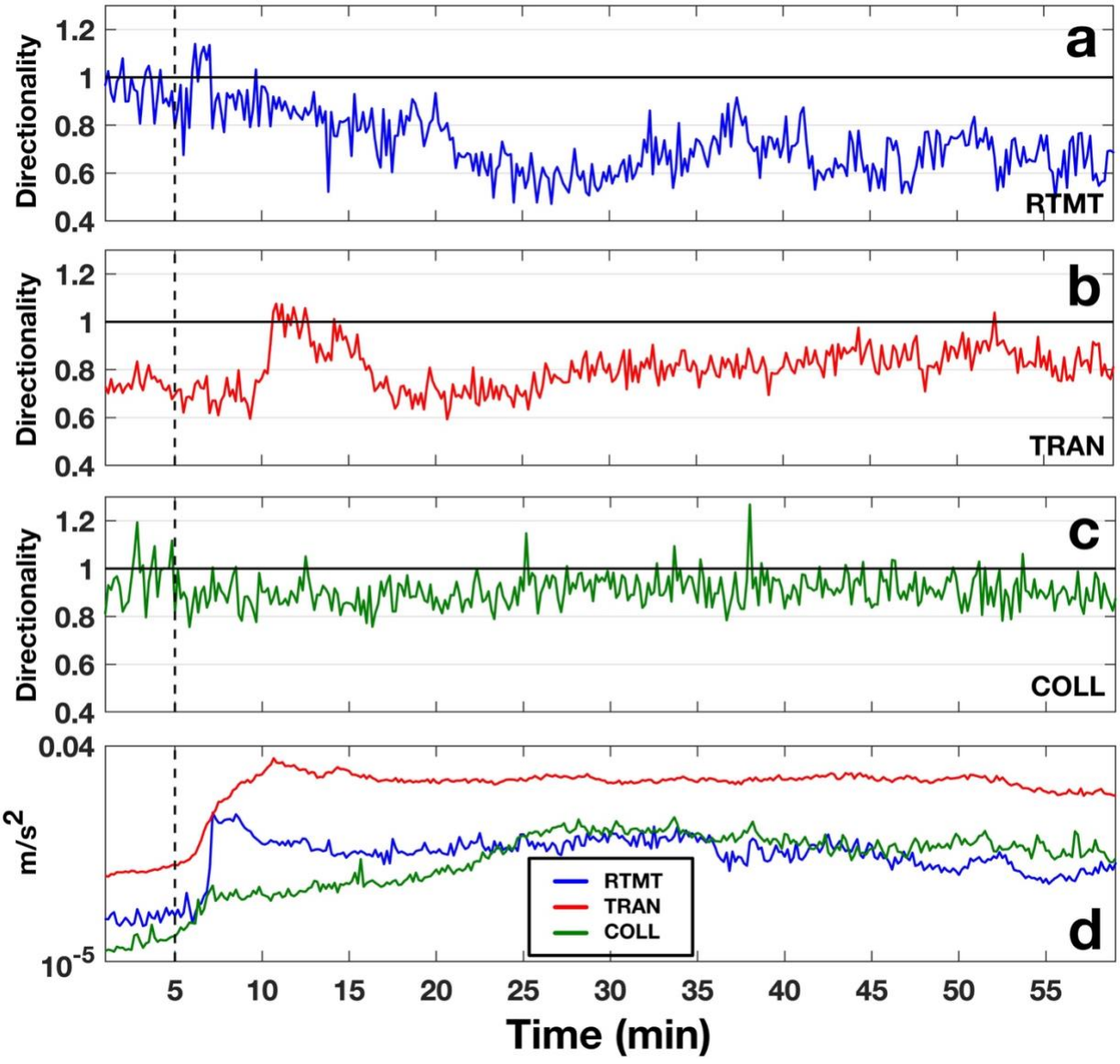


*Figure 6 Directionality ratio plots over time for RTMT (a), TRAN (b), and COLL (c). Vertical RMS seismic signals for the three stations are plotted in (d) where blue is RTMT, red is TRAN and green represents COLL. The dashed vertical lines mark the timing of the lahar front passing the monitoring station. All DRs and RMS amplitudes were calculated using 10 s time windows.*

## 4. Discussion

### 4.1 Frequency constraints

In order to obtain an understanding if PSFs are able to properly describe the lahar dynamics (i.e. the weight of the spectral amplitude at the PSF), frequency constraints must be analyzed. To complete this, normalized spectrograms along with spectral centroidal frequency (SCF) and spectral spreads are computed (e.g. Rubin et al., 2012; Saló et al., 2018). The normalized spectrograms are estimated by normalizing (using the maximum) the spectral amplitude for each 10 second time window of the lahar individually. By normalizing each time window, ranges of dominant frequencies can be visualized. SCFs are used because they represent the weighted average of the spectra, and yield the location (i.e. frequency) of the center of the spectral mass. The SCF of each time window is estimated similar to that of Saló et al. (2018), in which:

$$SCF = \frac{\sum_{f1}^{f2} f * A(f)}{\sum_{f1}^{f2} A(f)} \quad (1)$$

where *f* is the frequency and *A(f)* is the spectral amplitude associated with each frequency bin. The spectral spread measures the width of the spectral energy around the SCF (i.e. standard deviation), thus yielding information about the quality of the PSFs (e.g. Rubin et al., 2012; Giannakopoulos and Pikrakis, 2014; Saló et al., 2018) . Spectral spread can be estimated by:

$$SS = \sqrt{\frac{\sum_{f1}^{f2} (f - SCF)^2 * A(f)}{\sum_{f1}^{f2} A(f)}} \quad (2)$$

The computed normalized spectrograms along with SCFs and spectral spreads for each of the three monitoring stations are shown in Figure 7. For simplicity and comparison, only the flow parallel data are shown. The normalized spectrograms for every station and component can be seen in Figures S1-S3, as well as the values in Table S1.

The normalized spectrogram for RTMT (Figure 7a) yields very similar results to that of the PSF (Figure 3b), where most of the higher spectral amplitudes are at the same frequencies as those of the PSF. Notably, the low ~10 Hz signal immediately before the arrival of the head of the lahar is not only seen in the dominant normalized spectra, but also through the decrease in SCF. Additionally, the PSFs at these time windows are contained within the spectral spread (Figure 7a, black lines). For TRAN, the normalized spectrogram (Figure 7b) is again, very similar to the PSF in Figure 4b. The SCF mirrors the pattern of the PSF with higher frequencies for the streamflow, a decrease for the front of the lahar, increase for the head of the lahar, decrease after the passing of the head, and finally a slight increase later in the lahar body. The normalized spectra yields this same pattern, with the late lahar body displaying the only timeframe with increased spectral amplitude distributed throughout the spectral spread (Figure 7b, after 30 min). This most likely explains the bimodal distribution of PSFs for TRAN in Figure 4 after the ~30 min mark. Continuing, the normalized spectrogram for COLL (Figure 7c), also shows similarities to that of the PSFs in Figure 5b. The PSFs for COLL range between ~20-30 Hz with a slight bimodal pattern. This same pattern can be seen where the higher spectral amplitudes are located (Figure 7c). Furthermore, the SCF for COLL splits the PSF range and stays at ~25 Hz during the bimodal phase of the PSF. Overall, with the analysis of the normalized

spectrograms, SCFs and spectral spreads, we confirm that the use of PSFs to describe mass flow dynamics is concise for the 18 March 2007 lake-breakout lahar.

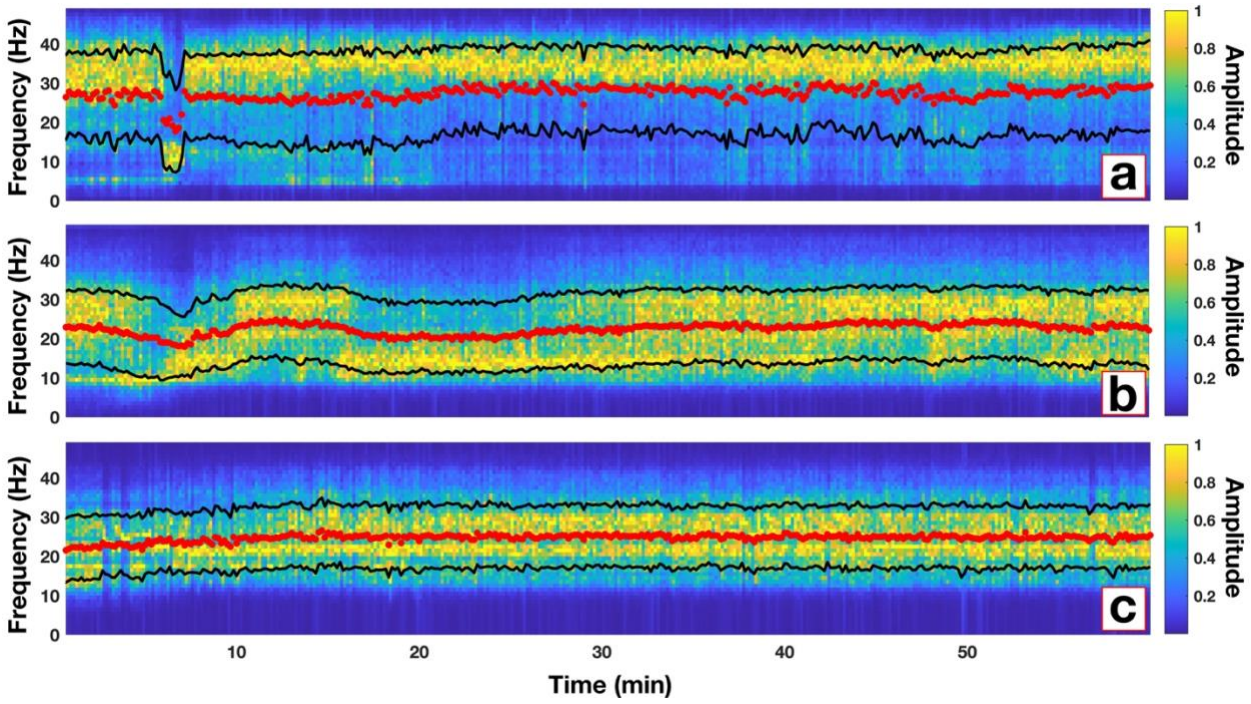


*Figure 7 Normalized spectrograms for the flow parallel direction for each of the three monitoring sites along the Whangaehu channel. Red dots represent the spectral centroidal frequency and black lines show the range of the spectral spread. Note, normalized spectrograms for the other directions can be seen in Figures S1-S3.*

## 4.2 Evolution of lahar signals

### *4.2.1 Phase 1 evolution*

A lahar propagating down channel can bulk up by collecting material from erosion or through the coalescing of multiple pulses to shorten the total length of the lahar (Procter et al., 2010; Doyle et al., 2011). Lahars can also debulk by depositional means or by the natural elongation of the lahar as it progresses down channel (Doyle et al., 2011; Lube et al., 2012). Considering the 18 March 2007 lake-breakout lahar was a large pulse of water that only mixed with the existing streamflow and contained no juvenile material, examining the seismic signatures along

330 the flow path can be used to characterize the evolution and transformation of a lake-breakout
331 event from outburst flood to hyperconcentrated flow and beyond. At RTMT, the seismic
332 signature is dominated by the flow parallel direction (Figure 3d) with > 30 Hz PSF (Figure 3b).
333 The exception to this is the timeframe immediately before the head of the lahar passes, when
334 the PSF decreases to ~10 Hz. This low frequency signal can be seen also at TRAN (Figure 4a-c)
335 and in the flow parallel direction at COLL (Figure 5b). However, at COLL the PSF is ~20 Hz
336 instead of 10 Hz as recorded at RTMT and TRAN, most likely due to differing flow properties at
337 83 km from source. This low PSF before the head of the lahar arrives at each station probably
338 represents the supercharged stream flow pulse (bow wave, Figure 2c) that is pushed in front of
339 the head of the lahar (i.e. phase 1, see section 1.1) as described by Cronin et al. (1999) where
340 they noticed these same pulses in front of lahar heads for three lahars on Mt. Ruapehu in 1995.
341 Conversely, this frontal pulse could be from the uplift of streamflow from the faster moving
342 underflow of the lahar (Manville et al., 2000). Furthermore, the low frequency zone before the
343 head of the flow lengthens as the lahar progresses downstream, suggesting that lahar
344 elongation can also be seen in the seismic frequency domain (~1 min at RTMT, ~5 min at TRAN).
345 The ~10 Hz PSF may be explained by flow processes (e.g. frictional resistance of the flow by the
346 channel, waves at free surface) (Schmandt et al., 2013; Barriere et al., 2015; Bartholomaus et
347 al., 2015) and could be due to the flow at this stage being more sensitive to discharge (e.g.
348 increase in shear velocity and/or flow depth) (Gimbert et al., 2014; Schmandt et al., 2017;
349 Anthony, et al., 2018) or in the case of the underflow hypothesis, frictional sliding on the
350 channel bed (Huang et al., 2004). The frontal surge or phase 1 of the lahar can be seen in the
351 DR (Figure 6) as well. For every station along the channel the DR has a slight drop when phase 1

passes the recording station (Figure 6, dashed line). The elongation of phase 1 also has a correlation with distance from source, where the dip in the DR lasts for only ~1 min at RTMT, ~5 min at TRAN, and approximately 20 min at COLL. The reason the DR decreases during phase 1 for the 2007 lahar could be due to the parallel component being more sensitive to flow processes than bedload forces (Barriere et al., 2015; Roth et al., 2016). During phase 1 discharge increases, sediment concentration is low (Cronin et al., 1999), and streamflow dominates resulting in a low DR (e.g. Doyle et al., 2010). The low DR can also be seen before the arrival of phase 1, due to streamflow already occurring in the channel. The higher flow parallel amplitude over cross-channel amplitude for streamflow has also been noted in the past for lahars at Volcán de Colima, Mexico (Walsh et al., 2020).

*4.2.2 Phase 2 evolution*

Following the low PSF phase 1 (i.e. front of the lahar), the peak seismic amplitude occurs (flow head). The peak seismic amplitude for RTMT (Figure 3d) is accompanied by an increase to higher PSFs > 30 Hz (Figure 3a-c, 7a). PSFs > 30 Hz have been shown in the past to be either dominated by turbulence or bedload transport (e.g. Gimbert et al., 2014; Roth et al., 2016). The 2007 lake-breakout lahar has been described as a hyperconcentrated streamflow (e.g. Procter et al., 2010b) with low sediment concentration, especially early on before the lake water captured enough material to bulk up and transform. At RTMT, which was only 7.4 km from source, the lahar had not fully bulked up yet and was in a net depositional regime (Procter et al., 2010a). Due to the conditions of the lahar at RTMT (e.g. Figure 2a), we surmise the higher PSF content for the peak seismic amplitude is dominated by turbulent-flow-induced noise.

Furthermore, the higher PSF content at RTMT (>30 Hz) compared to TRAN and COLL (~30 Hz) could be due to the angle of the slope at the recording stations. Gimbert et al. (2014) noted that turbulence noise will dominate over bedload-induced noise on steeper slopes due to an increase in shear velocity. If we use the average flow velocities as a comparison, the lahar at RTMT (9.3 m/s) flowed faster than at the other two stations (TRAN, 5.6 m/s; COLL, 4.8 m/s). Further down the channel at TRAN, the PSF for the peak seismic amplitude is ~30 Hz for all three components (Figure 4a-c, Table S1). Again, this high PSF may be attributed to turbulence, as seen by the images taken at TRAN (Figure 2d). The difference at TRAN is the duration of the higher PSF, where at RTMT the high PSF stays throughout the entirety of the recording window, at TRAN the high PSF only last for ~5 min (Figure 4a-c, ~11-16 min). The difference at TRAN could be from the evolution of the lahar. By time the lahar reached the monitoring station at TRAN (28 km from source) the lahar was fully bulked up and had the properties of a traditional four phase lahar as described by Scott (1988) or Cronin et al. (1999) (Figure 2c-e, see section 4.2.3). By time the lahar reached COLL 82 km from source (Figure 5), the peak seismic amplitude is associated with PSFs between 15-30 Hz, with bimodal patterns in the horizontal components and a tighter spread in the vertical component (~27-29 Hz). At COLL, the lahar had converted into a plug-like flow with lower turbulence and hence the higher PSFs are most likely associated with bedload transport (Figure 2f). Furthermore, Burtin et al. (2010) and Roth et al. (2016) noted that when the vertical component has greater seismic amplitudes than the horizontal components, bedload dominates. This same amplitude feature can be seen at COLL (Figure 5d, past ~25 min) where the vertical energy is greater than each of the horizontal components. The bimodal frequency pattern of the horizontal components (Figure 5a,b) is

likely to be the recording of both water-flow noise (lower PSF) and bedload transport (higher PSF). This also explains why the vertical component does not show the same bimodal frequency pattern. Barriere et al. (2015) described the parallel component as being more sensitive to flow properties (e.g. discharge, depth, shear velocity), and Doyle et al. (2010) noted that the cross-channel component is likely dominated by the amount of turbulence (water and particles acting on the channel walls), thus the reasoning behind the differing PSF patterns between components. This PSF feature is similar to the lahars recorded by Walsh et al. (2020), where the cross-channel PSF is confined within a narrow band around 15-20 Hz and the flow parallel PSF is more bimodal (10-40 Hz). At COLL, the cross-channel PSF (Figure 5a) is dominated by PSFs at ~18 Hz (lower than vertical component at ~28 Hz, Figure 5c), with the flow parallel between 20-30 Hz (Figure 5b).

The DR at the peak seismic amplitude for all three recording stations increases (Figure 6). The DR for both RTMT and TRAN increases to DR > 1. Doyle et al. (2010) noted that higher wetted perimeters will increase the DR, which can be seen at TRAN for the 18 March 2007 lake-breakout lahar (Figures 2d, 6 peak DR/RMS amplitude). Conversely, the DR decreases after the peak seismic amplitude while the wetted perimeter is still high (Figure 2d,e). While the wetted perimeter may be a factor in increasing cross-channel energy and thus the DR, the more likely explanation for the 18 March 2007 lahar might be the higher level of particle collisions and turbulence at the peak seismic amplitude. More turbulent particle collisions would increase the DR (e.g. Doyle et al., 2010) due to more lateral excitation within the flow and against the channel walls increasing the cross-channel signal. The increase in collisional energy also relates well with the PSF, as higher PSF correlates to an increase in the amount of interflow collisions

as shown by Huang et al. (2004), and may also explain the slight increase in DR overall when the PSF increases (Figure 8a). The DR for COLL (Figure 6c) during this same timeframe probably is not due to the amount of particle collisions due to the plug-like flow (Figure 2f), but rather the increase in sediment concentration (Figure 8c). As the sediment concentration increases at COLL the DR starts to increase as well (Figure 8b). Similar to Doyle et al. (2010), COLL yields a correlation between DR and sediment concentration ($R^2$=0.95, Figure 8b), where higher DRs indicate higher concentrations of sediment contained in the flow. Lastly, as noted above, DRs may correlate with PSF or at least indicate differing processes taking place within the flow (Figure 8a). Lower PSF would produce lower DRs because low PSF are more sensitive to water-flow processes (hence higher parallel energy), whereas higher PSFs would produce higher DRs due to higher PSF being dominated by sediment, particle collisions and turbulence (higher cross-channel energy) (Figure 8a).

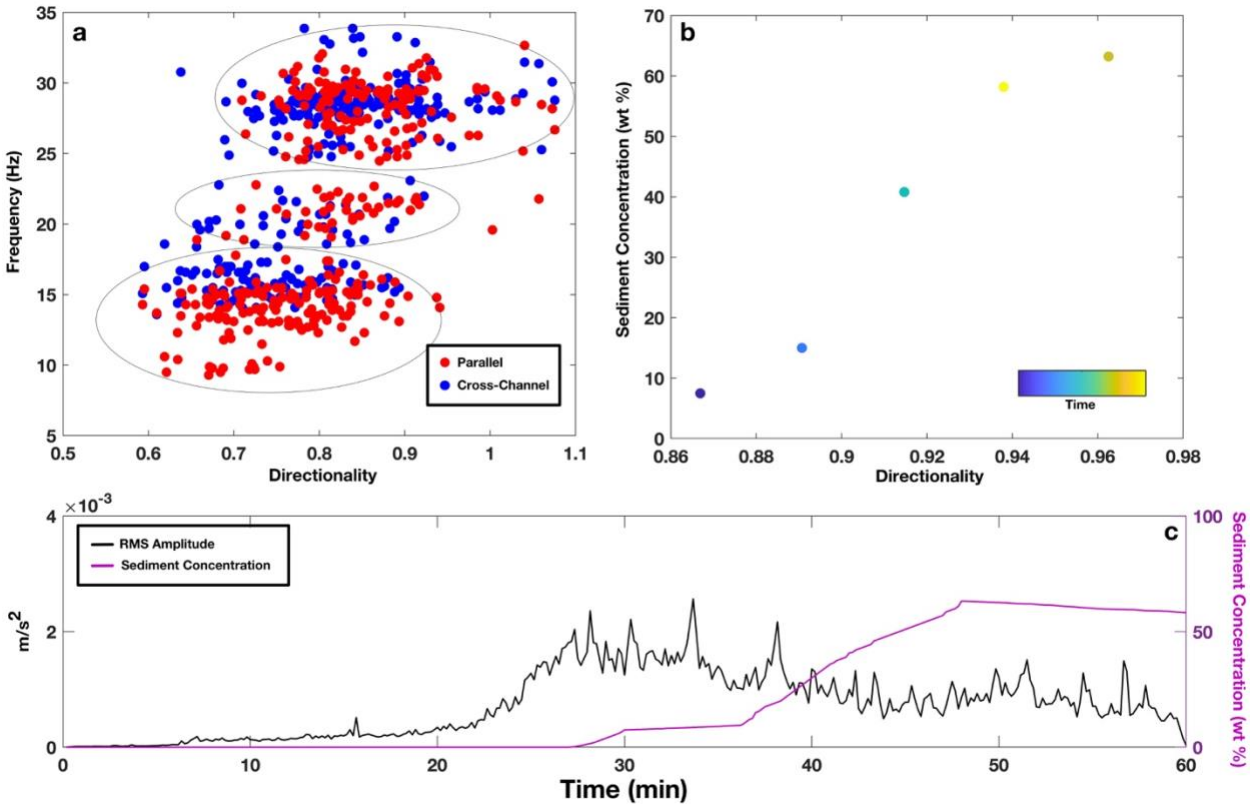


*Figure 8 Plots of (a) comparing PSF and DR at TRAN, (b) sediment concentration and DR at COLL ($R^2$=0.95), and (c) seismic amplitude (black line) with sediment concentration (purple line) depicting the lag in sediment at COLL. Note on (a) parallel (red dots) and cross-channel (blue dots) PSF display three different zones (black circles). Also note that at COLL the first sediment concentration measurement did not occur until the 30 min mark.*

### *4.2.3 Development of flow phases at TRAN*

While the lahar at RTMT was a large outburst flood/sediment-laden flow, and at COLL a plug-like flow, at TRAN the 18 March 2007 lahar was a dynamic bulked up lahar (see Figure 2b-e). The evidence for this is in the PSF content for TRAN (Figure 4a-c) compared to the other two monitoring sites (Table S1). At TRAN the PSF has a step-up step-down pattern for the first 30 min of the lahar passing, and then transitions to a bimodal or wide PSF range for the rest of the recording window. As noted above, the low PSF preceding the lahar head arrival is thought to be due to a sensitivity to water transport properties (Figure 2c, phase 1). The increase to higher PSFs during the peak seismic amplitude may be from particle collisions and/or higher

turbulence (Figure 2d, transition from phase 1 to 2). After the maximum seismic amplitude at TRAN (Figure 4, ~10-15 min), the PSF decreases to 10-20 Hz. This drop in PSF after the highest stage and amplitude could be from a more water-flow dominate regime (seen in the increased parallel amplitude, Figure 4d, and decrease in DR, Figure 6b), where turbulence decreases (Figure 2e), discharge is still high, and the peak sediment concentration has not occurred yet (e.g. Cronin et al., 1999). Likewise, the decrease may also be from greater frictional sliding on the channel bed (Huang et al., 2004). After the decrease to 10-20 Hz PSFs, the PSF displays a bimodal or wide frequency range at ~28 min (Figure 4a-c, 7b). As aforementioned for COLL, this PSF pattern could be from both bedload- and water-flow-induced noise. This timeframe (phase 3) is also where the peak sediment concentration would be (not recorded at TRAN), as noted by Cronin et al. (1999), and thus the PSF would show more bedload high PSF. This hypothesis also compares well with the DR (Figure 6b), where the cross-channel energy increases starting at ~25 min indicating that the sediment concentration may be increasing (Doyle et al., 2010). Finally, the wide PSF range later in the recording window (Figure 4) could also result from the lahar having two distinct layers as described by Cronin et al. (2000), where there is a wide more dilute finer grain top layer and a channelized sediment-rich layer on the bottom. The two layer model can apply to TRAN because the lahar at this monitoring station overtook the channel (Figure 2d,e) and proceeded to flow horizontally outward forming the surface layer described by Cronin et al. (2000).

### 4.3 Implications for monitoring

The main goal of this research is to contribute in defining better monitoring criteria for dangerous mass flow events. The data described above is part of a larger collection of monitoring data collected over the entire length of the Whangaehu channel consisting of 21 monitoring sites and years of preparation (e.g. Manville and Cronin, 2007; Keys and Green, 2008). Due to this, the ability to accurately estimate the properties of the lahar at various stages along its path is possible. When it comes to flow events of any size, the ability to understand how the dynamics change with distance along the channel is important for warning and future hazard mitigation. We show here that a lake-breakout event can start out as an outburst flood, bulk up into a hyperconcentrated flow, then eventually elongate and entrap enough sediment to transform into a plug-like slurry flow. Each of these flow types yields differing PSF ranges and patterns due to the relationship between the channel geometry, sediment concentration, turbulence, and bedload transport. While the lahar at different stations along the channel may have differing PSF content, we also show that the lahar elongates and a predictable model (e.g. Cronin et al., 1999) can be used with and shown in the seismic data. Being able to apply such a model may yield some relevance of universality in terms of warning systems at different distances away from the mass flow source. Whereas, shown above, the flow phases at each monitoring station can be seen, but at differing lengths and times in the seismic signal (e.g. Figure 6). To better visualize this concept, conceptual models based off of the Cronin et al. (1999) models are created for each of the three seismic stations for the 18 March 2007 lahar (Figure 9). In the conceptual models for the 2007 lahar, the aforementioned elongation of the frontal pulse or bow wave (phase 1) and head of the

484 lahar (phase 2) is shown, along with the differences and similarities between the properties of

485 the lahar at the three seismic monitoring sites.

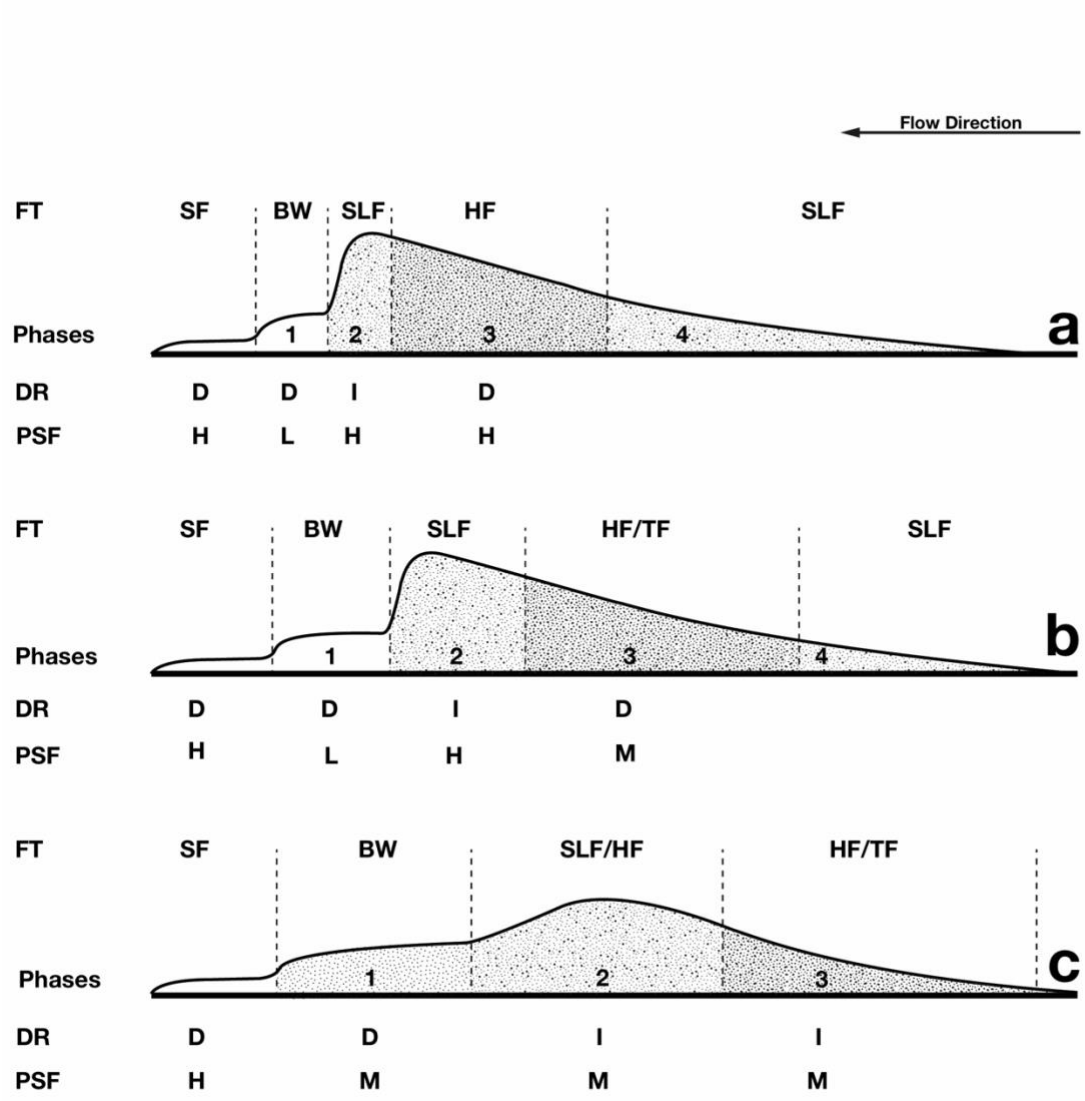


486

487 *Figure 9 Conceptual models for the 18 March 2007 lahar at each of the three monitoring stations along the*
488 *Whangaehu channel depicting flow type and the estimated seismic properties at each flow phase. a) RTMT 7.4 km*
489 *from source, b) TRAN 28 km from source, and c) COLL 83 km from source. Flow types (FT) are as followed;*
490 *streamflow (SF), bow wave streamflow (BW), hyperconcentrated flow (HF), Transitional flow (TF), and sediment-*
491 *laden streamflow (SLF). Note, decreased (D), increased (I), high (H), low (L), and mixed (M) are notations for*
492 *directionality ratios and peak spectral frequency estimates. See Table S1 for value ranges for each property.*

493 Another implication for future warning is the implementation of 3-component sensors and the

494 use of DRs for channels that have streamflow. Walsh et al. (2020) showed for lahars flowing in

La Lumbre channel at Volcán de Colima that the DR for streamflow is <1 and then increases when the head of the lahar arrives. This same feature can be seen at each of the three monitoring sites for the 18 March 2007 event (Figure 6) indicating differing flow types will still show this DR pattern within the same flow and at other channels. To further show this, there were three natural non-lake-breakout eruption-based lahars that occurred in the Whangaehu channel in September 2007 (for more details on the lahars see Cole et al., 2009; Kilgour et al., 2010) and recorded on the seismometer at RTMT. The DR for the September events starts with streamflow with a DR < 1 and when the first lahar arrives the DR increases to >1 and as the lahar fully passes, the DR decreases to <1 again (Figure 10a). As the second lahar arrives at RTMT (Figure 10, second dashed line), the DR increases to >1 again. After the second lahar passes the DR deceases once again back below DR<1. Finally, as the third lahar arrives (Figure 10, third dashed line) the DR yet again increases above 1 for the entirety of the event.

For many mass flows and especially those that flow into channels with preexisting streamflow, the peak seismic amplitude does not always coincide with the arrival of the mass flow, and thus may not be the most reliable for event detection or warning (e.g. Arratano and Moia, 1999; Cole et al., 2009). These observations may be due to a frontal surge, the lag in sediment concentration or differences in peak amplitude with peak discharge. Phase 1 (frontal streamflow surge) of the model proposed by Cronin et al. (1999) was based on a hyperconcentrated flow interacting with streamflow, but has also been shown for debris flows as well (e.g. Arratano and Moia, 1999). Arratano and Moia (1999) showed at Moscardo Torrent, Italy, through a hydrograph that there was a precursory surge ahead of the debris flow that was not seen in the seismic record. Similarly, at Ruapehu, for the 18 March 2007 lahar, at each of

517 the three stations there is little evidence or rise in the seismic amplitude that would indicate
518 that there was a precursory surge or phase 1 (Figures 3-5, bottom panel), which could be
519 problematic for detection methods that use amplitude thresholds or short-time-average vs
520 long-time-average (STA/LTA) algorithms. Conversely, the surge ahead of the lahar can be seen
521 in both the PSF analysis (drop to low frequencies) and in the DR (decrease in DR) right before
522 the peak seismic amplitude arrives. This shows that when monitoring for future events that not
523 only the amplitude should be used, but other analysis (e.g. PSF, DR) as well, otherwise there
524 could be a delay in the detection of an event.

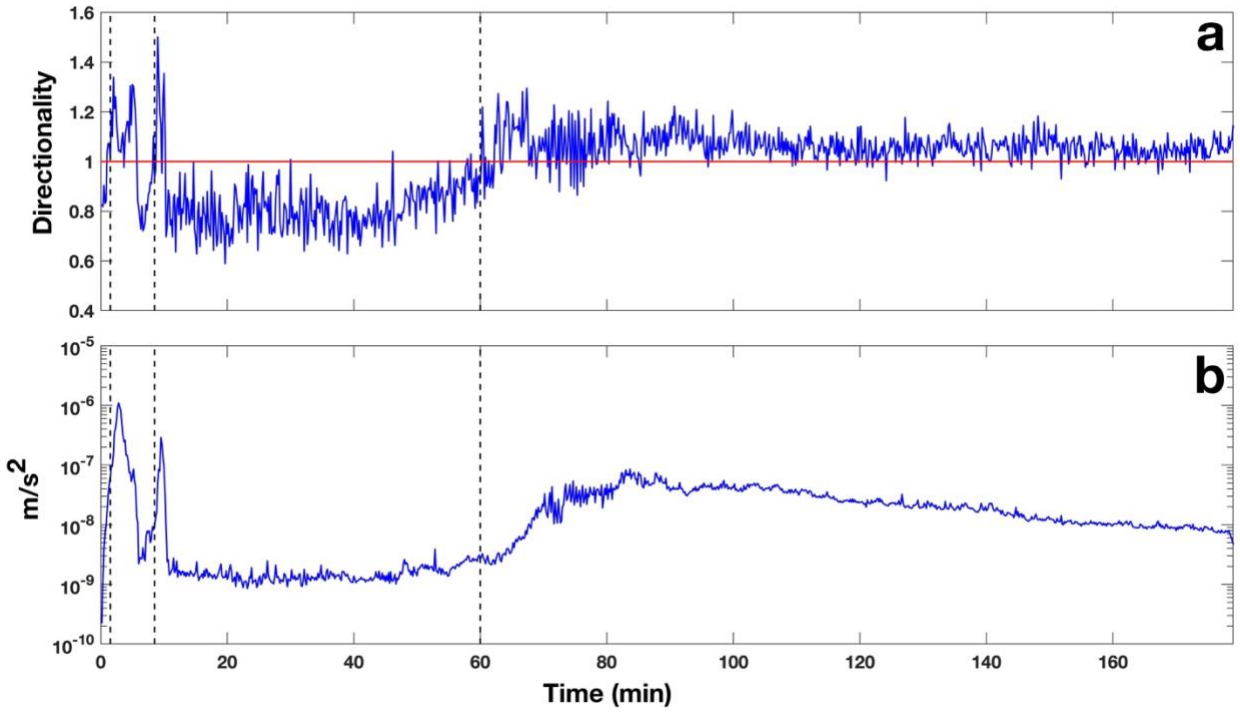

525

526 *Figure 10 (a) Directionality ratio for the time sequence of the three lahars that occurred on 25 September 2007. (b)*
527 *RMS amplitude of the seismic record at RTMT during the timing of the three September lahars. Note that the black*
528 *dashed lines represent the timing of each lahar arriving at the monitoring site.*

529 Using all three components of the seismometer can be very beneficial in lahar monitoring. The
530 above-mentioned DR analysis can only be completed with horizontal recording, and analyzing

PSF in each component can yield critical information about the flow properties and dynamics. Examining the seismic amplitude differences can generate significant discoveries, for example, when the vertical component is stronger than the horizontal components, bedload may dominate over turbulence noise (Burtin et al., 2010). Greater flow parallel signals may indicate higher water transport noises (Barrier et al., 2015), while higher cross-channel signals could be caused by increased interflow particle collisions and flow-channel wall interactions (Doyle et al., 2010). While using the differences in each component can be useful, there are also some concerns. Channel geometry and bed conditions can alter the seismic signal (e.g. Coviello et al., 2019; Marchetti et al., 2019). Additionally, the flow parallel direction can be influenced by the lahar that has already passed, the lahar at the station and the lahar arriving. Furthermore, the tilt of the seismometer may play a large role in determining which component is stronger (e.g. Anthony et al., 2018). In the case of the 18 March 2007 lahar a large pulse of water passed the monitoring stations which may explain why the parallel component is stronger than the other two components at RTMT (Figure 3d) and TRAN (Figure 4d). At COLL, the lahar had elongated, lost energy, and thus shows more decreased flow parallel energy compared to the previous two stations (Figure 5d). In the cross-channel direction, if a flow overtops the channel, the amplitude would presumably be dampened. This may be the case at TRAN where both the flow parallel and vertical directions are more energetic than the cross-channel amplitude after the passing of the head and breaking out of the channel occurred (Figures 2d, 4d). Another concern when using the horizontal components of a seismometer are the effects shallow layers may have on the site response of the sensor. This is especially true when a sensor is installed on soft or lose sediment (e.g. soil, fluvial/alluvial deposits). To test for potential effects by shallow layer

553 fundamental frequencies, H/V analysis of ambient noise (streamflow dominant) was conducted
554 (see Supplementary material). For RTMT, the H/V results depict a broad frequency peak
555 between 5-15 Hz with a local maximum at ~8 Hz (Figure S4a). Comparing the H/V frequency
556 with the PSF of RTMT (Figure 3), the only overlap is when the front of the lahar passes the
557 station where the PSF decreases for ~1 minute before the head of the lahar arrives. The H/V
558 analysis for TRAN has a multi-broad-peak shape, with frequency peaks at ~14 and ~28-35 Hz
559 (Figure S4b). While these frequencies are similar to PSF values for TRAN (Figure 4), the H/V
560 analysis has no distinguishable fundamental frequency, contains large error, and no frequency
561 peak has a H/V amplification > 2. In order for a H/V frequency peak to be considered ideal,
562 generally the amplification must be greater than 2 and the standard deviation lower than a
563 factor of 2 (SESAME, 2004). The H/V amplification for COLL displays a broad frequency peak
564 between 13-18 Hz, with a local maximum at ~18 Hz (Figure S4c). Comparing the PSFs at COLL
565 (Figure 5), only the cross-channel direction has significant PSF values in the same frequency
566 range (~18 Hz band). With all three stations not yielding distinct H/V fundamental frequencies,
567 we surmise that the PSF content for the 18 March 2007 lake-breakout lahar is most likely
568 dominated by the large flow passing by the seismic sensor rather than large site amplification
569 effects from a shallow layer. While this may be the case, there is still the possibility that some
570 of the PSF values could be due to local effects and should not be considered in the lahar
571 analysis, e.g., the low PSFs at RTMT between 15-20 min (Figure 3a,b), at TRAN contributing to
572 some of the “jumping” in PSF content (Figure 4a-c), or in the mostly dominant 15-20 Hz PSF in
573 the cross-channel direction at COLL (Figure 5a). Conversely, SCF values at each station do not
574 reside in the broad H/V frequency range at any station (Figure 7), which may further support

575 the hypothesis that almost all of the recorded frequencies are indeed produced by the lahar.
576 With the use of horizontal components becoming common in mass flow monitoring, future 3-
577 component analyses of mass flows should consider estimating H/V ratios or use other site
578 response methods (e.g. spectral ratio analysis) in order to identify whether near-surface
579 structures may affect the recorded flow data. Overall, all these concerns can and should be
580 tested to estimate potential error in 3-component methods. Nevertheless, using all three
581 components of the seismometer can enhance the productivity of warning systems, and if
582 possible, should be used instead of single component sensors.

583 Finally, implementation of these new results into new or existing mass flow warning systems
584 must be discussed. In an ideal setup, to remove any doubt about the recorded signal, machine
585 learning techniques should be used to separate the mass flow noise from other non-flow noises
586 (e.g. environmental, human induced, earthquakes). For instance, recently Wenner et al. (2021)
587 used a supervised random forest algorithm to classify differing sources in a debris flow setting.
588 Once the mass flow source has been classified, integrating automated DR and PSF analysis
589 would be quick and straightforward. Implementation of these techniques would be similar to
590 other seismic analysis or detection methods, such as a STA/LTA (e.g. Coviello et al., 2019) or a
591 number of frequency detection algorithms (e.g. Rubin et al., 2012) where real-time analysis of
592 set time windows are used to determine if there has been a change in the seismicity along the
593 channel. The system could be programed to identify changing features in the flow automatically
594 by analyzing the content of each window, as well as comparing previous time windows. The
595 analysis of continual data could then be feed into machine learning algorithms (e.g. Rubin et al.,
596 2012; Wenner et al., 2021) to increase the confidence of not only detection, but the

characterization of flow behavior. One of the main discoveries of this research was the evolution of seismic signals produced by the lahar as the flow moved further from its source. The changes in the seismic signal along with the flow characteristics may be able to help hazard and forecast modeling through the use of numerical models (e.g. Mead et al., 2021). Modern flow hazard assessment is based on numerical models that use potential energy equations of a large non-changing mass sliding down slope with limited inputs for how the flow may evolve over time as starting inputs. This can lead to errors in risk mitigation and hazard assessments. The findings shown above on how the 18 March 2007 lahar evolved over 83 km at Mt. Ruapehu will help to improve mass flow modeling in the future by enabling modelers to add constrains or more inputs on how a mass flow might evolve, leading to improved forecasts and hazard assessment.

## 5. Conclusions

At 23:18 UTC on 18 March 2007, Mt. Ruapehu produced the biggest lahar in New Zealand in over 100 years causing $1.3 \times 10^6$ $m^3$ of water to flow out of the Crater Lake and rush down the Whangaehu channel flowing for over 200 km to the Tasman sea. Seismic analysis at three monitoring locations along the channel (7.4, 28, and 83 km) yielded an understanding of how flow type and processes of the lahar evolve with distance. The proximal lahar was a highly turbulent outburst flood, which generated high PSF content in all three components. Further along the channel after the lahar had bulked up and transformed into a multi-phase hyperconcentrated flow, the PSF content was variable and showed changes in the flow regime/phase. Finally, at the most distal monitoring station, the lahar had lost energy and

transformed into a slurry-type flow where the PSF content became more bedload-dominant. Additionally, directionality ratios from all three sites along with data from additional lahars yielded strong evidence that DRs can be used for warning systems when there is streamflow present in the channel. Furthermore, PSF and DRs show evidence of a pre-lahar water pulse that may be concealed in the raw seismic data, but has been observed visually. Ultimately, the use of 3-component broadband seismic analysis for the 18 March 2007 lahar at Mt. Ruapehu may lead to more accurate and advanced real-time warning systems for mass flows through the use of frequency and directionality around the world.

*Author Contribution*

BW performed seismic analysis and drafted the manuscript, CL organized and prepared data, and JP created the visual location representation of the event. All participating authors contributed to the discussions and editing of the draft of the manuscript, as well as approving the final edition.

*Competing Interests*

The authors declare that they have no conflict of interest

*Data Availability*

The data used in this publication can be found at: Braden Walsh; Charline Lormand; Jon Procter; Glyn Williams-Jones (2022), "18 March 2007 Mt. Ruapehu lahar seismic data," https://theghub.org/resources/4890.

*Acknowledgements*

This work was supported by the Resilience to Natures Challenges – New Zealand National Science, volcano program of research. We would also like to thank all the people from Massey University, Horizons Regional Council, NIWA, and the Department of Conservation that collected data and set up monitoring locations all along the channel in preparation for and during the lahar. A final special thanks to Kate Arentsen for editorial support.

## References

Anthony, R., Aster, R., Ryan, S., Rathburn, S., Baker, M.: Measuring mountain river discharge using seismographs emplaced within the hyporheic zone, *Journal of Geophysical Research: Earth Surface, 123, 210-228, 2018.*

Arattano, M., Marchi, L.: Measurements of debris flow velocity trough cross-correlation of instrumentation data, *Natural Hazards and Earth System Sciences, 5, 137-142, 2005.*

Arattano, M., Marchi, L., Genevios, R., Berti, M, Simoni, A., Tecca, P., Bonte, M.: Field monitoring and real time management of debris flows, *European Project "Debris Flow Risk" (N.ENV4960253), Final Report, 30, 1999.*

Arattano, M., Moia, F.: Monitoring the propagation of debris flow along a torrent, *Hydrological Sciences- Journal des Sciences Hydrologiques, 44(5), 811-823, 1999.*

Barriere, J., Oth, A., Hostache, R., Krein, A.: Bed load transport monitoring using seismic observations in a low-gradient rural gravel bed stream, *Geophys. Res. Lett., 42, 2294-2301, 2015.*

Bartholomaus, T., Amundson, J., Walter, J., O'Neel, S., West, M., Larsen, C.: Subglacial discharge at tidewater glaciers revealed by seismic tremor, *Geophys. Res. Lett., 42, 6391-6398, 2015.*

Burtin, A., Vergne, J., Rivera, L., Dubernet, P.: Location of river-induced seismic signal from noise correlation functions, *Geophys. J. Int., 182, 1161-1173, 2010.*

Capra, L., Borselli, L., Barley, N., Ruiz, J., Norini, G., Sarocchi, D., Caballero, L., Cortes, A.: Rainfall-triggered lahars at Volcan de Colima, Mexico: Surface hydro-repellency as initiation process, *Journal of Volcanology and Geothermal Research, 198, 105-117, 2010.*

Capra, L., Coviello, V., Borselli, L., Marquez-Ramirez, V., Arambula-Mendoza, R.: Hydrological control of large hurricane-induced lahars: evidence from rainfall-runoff modeling, seismic and video monitoring, *Nat. Hazards Earth Syst. Sci., 18, 781-794, 2018.*

Carrivick, J., Manville, V.: A fluid dynamics approach to modelling the 18$^{th}$ March 2007 lahar at Mt. Ruapehu, New Zealand, *Bull. Volcanol., 71, 153-169, 2009.*

Cole, S., Cronin, S., Sherburn, S., Manville, V.: Seismic signals of snow-slurry lahars in motion: 25 September 2007, Mt Ruapehu, New Zealand, *Geophys. Res. Lett., 36, L09405, 2009.*

Coviello, V., Arattano, M., Comiti, F., Macconi, P., Marchi, L.: Seismic characterization of debris flows: Insights into energy radiation and implications for warning, *Journal of Geophysical Research: Earth Surface, 124, 2019.*

Coviello, V., Capra, L., Vazquez, R., Marquez-Ramirez, V.: Seismic characterization of hyperconcentrated flows in a volcanic environment, *Earth Surf. Process. Landforms., 43, 2219-2231, 2018.*

Cronin, S., Neall, V., Jerome, L., Palmer, A.: Unusual “snow slurry” lahars from Ruapehu volcano, New Zealand, September 1995, *Geology, 24, 1107-1110, 1996.*

Cronin, S., Neall, V., Jerome, L., Palmer, A.: Dynamic interactions between lahars and stream flow: A case study from Ruapehu volcano, New Zealand, *GSA Bulletin, 111(1), 28-38, 1999.*

Cronin, S., Neall, V., Jerome, L., Palmer, A.: Transformation, internal stratification, and depositional processes within a channelized, multi-peaked lahar flow, *New Zealand Journal of Geology and Geophysics, 43, 117-128, 2000.*

Doyle, E., Cronin, S., Cole, S., Thouret, J.: The coalescence and organization of lahars at Semeru volcano, Indonesia, *Bull. Volcanol., 72, 961-970, 2010.*

Doyle, E., Cronin, S., Cole, S., Thouret, J.: Defining conditions for bulking and debulking in lahars, *GSA Bulletin, 123, 1234-1246, 2011.*

Huang, C., Shieh, C., Yin, H.: Laboratory study of the underground sound generated by debris flows, *Journal of Geophysical Research, 109, F01008, 2004.*

Iguchi, M.: Proposal of estimation method for debris flow potential considering eruptive activity, *Journal of Disaster Research, 14(1), 126-134, 2019.*

Giannakopoulos, T., Pikrakis, A.: Introduction to Audio Analysis, Chapter 4- Audio Features, *Academic Press, 59-103, 2014, https://doi.org/10.1016/B978-0-08-099388-1.00004-2.*

Gimbert, F., Tsai, V., Lamb, M.: A physical model for seismic noise generation by turbulent flow in rivers, *Journal of Geophysical Research: Earth Surface, 119, 2209-2238, 2014.*

696 Keys, H., Green, P.: Ruapehu lahar New Zealand 18 March 2007: Lessons for hazard assessment
697 and risk mitigation 1995-2007, *Journal of Disaster Research, 3(4), 284-296, 2008.*

698 Kilgour, G., Manville, V., Della Pasqua, F., Graettinger, A., Hodgson, K., Joly, G.: The 25
699 September 2007 eruption of Mount Ruapehu, New Zealand: Directed ballistics, surtseyan jets,
700 and ice-slurry lahars, *Journal of Volcanology and Geothermal Research, 191, 1-14, 2010.*

701 Kogelnig, A., Surinach, E., Vilajosana, I., Hubl, J., Sovilla, B., Hiller, M., Dufour, F.: On the
702 complementariness of infrasound and seismic sensors for monitoring snow avalanches, *Nat.*
703 *Hazards Earth Syst. Sci., 11, 2355-2370, 2011.*

704 Kuehnert, J., Mangeney, A., Capdeville, Y., Vilotte, J., Stutzmann, E., Chaljub, E., et al.: Locating
705 rockfalls using inter-station ratios of seismic energy at Dolomieu crater, Piton de la Fournaise
706 volcano, *Journal of Geophysical Research: Earth Surface, 126, e2020JF005715, 2021.*

707 Lube, G., Cronin, S., Manville, V., Procter, J., Cole, S., Freundt, A.: *Geology, 40, 475-478, 2012.*

708 Manville, V., Cronin, S.: Breakout lahar from New Zealand's crater lake, *EOS Transactions,*
709 *88(43), 441-456, 2007.*

710 Manville, V., White, J., Hodgson, K.: Dynamic interactions between lahars and stream flow: A
711 case study from Ruapehu volcano, New Zealand: Discussion and reply discussion, *GSA Bulletin,*
712 *112(7), 1149-1152, 2000.*

713 Marchetti, E., Walter, F., Barfucci, G., Genco, R., Wenner, M., Ripepe, M., McArdell, B., Price, C.:
714 Infrasound array analysis of debris flow activity and implications for early warning, *Journal of*
715 *Geophysical Research: Earth Surface, 124, 567-587, 2019.*

716 Massey., C., Manville, V., Hancox, G., Keys, H., Lawrence, C., McSaveney, M.: Out-burst flood
717 (lahar) triggered by retrogressive landsliding, 18 March 2007 at Mt Ruapehu, New Zealand – a
718 successful early warning, *Landslides, 7, 303-315, 2010.*

719 Mead, S., Procter, J., Kerezturi, G.: Quantifying location error to define uncertainty in volcanic
720 mass flow hazard simulations, *Nat. Hazards Earth Syst. Sci., 21, 2447-2460, 2021.*

721 O'Connor, J., Clague, J., Walder, J., Manville, V., Beebee, R.: Outburst Floods, *Reference Module*
722 *in Earth Systems and Environmental Sciences, Elsevier, 2020.*

723 O'Shea, B.: Ruapehu and the Tangiwai disaster, *NZ J. Sci. Tech. 36B, 174-189, 1954.*

724 Pardo, N., Cronin, S., Palmer, A., Nemeth, K.: Reconstructing the largest explosive eruptions of
725 Mt. Ruapehu, New Zealand: Lithostratigraphic tools to understand subplinian-plinian eruptions
726 at andesitic volcanoes, *Bull. Volcanol., 74, 617-640, 2012.*

727 Pierson, T., Janda, R., Thouret, J., Borrero, C.: Perturbation and melting of snow and ice by the
728 13 November 1985 eruption of Nevado del Ruiz, Colombia, and consequent mobilization, flow
729 and deposition of lahars, *J. Volcanol. Geotherm. Res., 41(1), 17-66, 1990.*

730 Pierson, T., Scott, K.: Downstream dilution of a lahar: Transition from debris flow to
731 hyperconcentrated streamflow, *Water Resources Research, 21(10), 1511-1524, 1985.*

732 Procter, J., Cronin, S., Fuller, I., Lube, G., Manville, V.: Quantifying the geomorphic impacts of a
733 lake-breakout lahar, Mount Ruapehu, New Zealand, *Geology, 38, 67-70, 2010.*

Procter, J., Cronin, S., Sheridan, M.: Evaluation of Titan2D modelling forecasts for the 2007 Crater Lake break-out lahar, Mt. Ruapehu, New Zealand, *Geomorphology, 136, 95-105, 2012.*

Procter, J., Cronin, S., Fuller, I., Sheridan, M., Neall, V., Keys, H.: Lahar hazard assessment using Titan2D for an alluvial fan with rapidly changing geomorphology: Whangaehu River, Mt. Ruapehu, *Geomorphology, 116, 162-174, 2010.*

Procter, J. N., Cronin, S. J., Zernack, A. V., Lube, G., Stewart, R. B., Nemeth, K., & Keys, H.: Debris flow evolution and the activation of an explosive hydrothermal system; Te Maari, Tongariro, New Zealand. *Journal of Volcanology and Geothermal Research*, *286*, 303-316, 2014.

Procter, J., Zernack, A., Mead, S., Morgan, M., & Cronin, S.: A review of lahars; past deposits, historic events and present-day simulations from Mt. Ruapehu and Mt. Taranaki, New Zealand. *New Zealand Journal of Geology and Geophysics*, *64*(2-3), 479-503, 2021.

Roth, D., Brodsky, E., Finnegan, N., Rickenmann, D., Turowski, J., Badoux, A.: Bed load sediment transport inferred from seismic signals near a river, *J. Geophys. Res. Earth Surf., 121, 725-747, 2016.*

Rubin, M., Camp, T., Van Herwijen, A., Schweizer, J.: Automatically detecting avalanche events in passive seismic data, *11th International Conference on Machine Learning and Applications, , IEEE, 1, 13-20, 2012.*

Schimmel, A., Coviello, V., Comiti, F.: Debris-flow velocity and volume estimations based on seismic data, *Natural Hazards and Earth System Sciences, 2021.*

753 Schmandt, B., Aster, R., Scherler, D., Tsai, V., Karlstrom, K.: Multiple fluvial processes detected
754 by river side seismic and infrasound monitoring of a controlled floor in the Grand Canyon,
755 *Geophys. Res. Lett., 40(18), 4858-4863, 2013.*

756 Schmandt, B., Gaeuman, D., Stewart, R., Hansen, S., Tsai, V., Smith, J.: Seismic array constraints
757 on reach-scale bedload transport, *Geology, 45, 299-302, 2017.*

758 Saló, L., Corminas, J., Lantada, N., Mata, G., Prades, A., Ruiz-Carulla, R.: Seismic energy analysis
759 as generated by impact and fragmentation of single-block experimental rockfalls*, Journal of*
760 *Geophysical Research: Earth Surface, 123, 1450-1478, 2018.*

761 Scott, K.: Origins, behavior, and sedimentology of lahars and lahar runout flows in the Toutle-
762 Cowlitz river system, *USGS Professional Paper, 1988.*

763 Surinach, E., Vilajosana, I., Khazaradze, G., Biescas, B., Furdada, G., Vilaplana, J.: Seismic
764 detection and characterization of landslides and other mass movements, *Natural Hazards and*
765 *Earth System Sciences, 5, 791-798, 2005.*

766 Walsh, B., Coviello, V., Capra, L., Procter, J., Marquez-Ramirez, V.: Insights into the internal
767 dynamics of natural lahars from analysis of 3-component broadband seismic signals at Volcán
768 de Colima, Mexico, *Front. Earth Sci. 8, 542116, 2020.*

769 Walsh, B., Jolly, A., Procter, J.: Seismic analysis of the 13 October 2012 Te Maari, New Zealand,
770 lake breakout lahar: Insights into flow dynamics and the implications on mass flow monitoring,
771 *J. Volcanol. Geotherm. Res., 324,144-155, 2016.*

772 Wenner, M., Hibert, C., Van Herwijnen, A., Meier, L., Walter, F.: Near-real-time automated
773 classification of seismic signals of slope failures with continuous random forests, *Nat. Hazards*
774 *and Earth Syst. Sci., 21(1), 339-361, 2021.*